

# Lab on a Chip

Accepted Manuscript

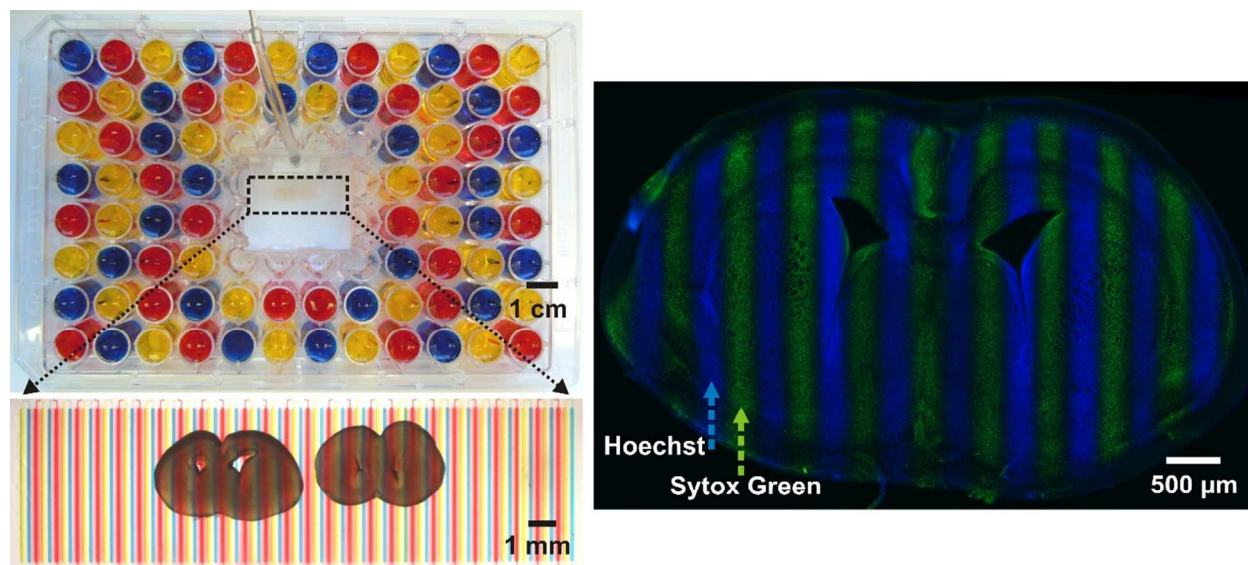


This is an *Accepted Manuscript*, which has been through the Royal Society of Chemistry peer review process and has been accepted for publication.

*Accepted Manuscripts* are published online shortly after acceptance, before technical editing, formatting and proof reading. Using this free service, authors can make their results available to the community, in citable form, before we publish the edited article. We will replace this *Accepted Manuscript* with the edited and formatted *Advance Article* as soon as it is available.

You can find more information about *Accepted Manuscripts* in the [Information for Authors](#).

Please note that technical editing may introduce minor changes to the text and/or graphics, which may alter content. The journal's standard [Terms & Conditions](#) and the [Ethical guidelines](#) still apply. In no event shall the Royal Society of Chemistry be held responsible for any errors or omissions in this *Accepted Manuscript* or any consequences arising from the use of any information it contains.



A 96-well plate-based microfluidic device enables multiplexed delivery of soluble molecules to organotypic tissue slices.

## ARTICLE

## Parallel Microfluidic Chemosensitivity Testing on Individual Slice Cultures

Cite this: DOI: 10.1039/x0xx00000x

Tim C. Chang<sup>a</sup>, Andrei M. Mikheev<sup>b</sup>, Wilson Huynh<sup>a</sup>, Raymond J. Monnat, Jr.<sup>c</sup>, Robert C. Rostomily<sup>b</sup>, and Albert Folch<sup>\*a</sup>

Received 00th January 2012,

Accepted 00th January 2012

DOI: 10.1039/x0xx00000x

[www.rsc.org/](http://www.rsc.org/)

There is a critical unmet need to tailor chemotherapies to individual patients. Personalized approaches could lower treatment toxicity, improve the patient's quality of life, and ultimately reduce mortality. However, existing models of drug activity (based on tumor cells in culture or animal models) cannot accurately predict how drugs act in patients in time to inform the best possible treatment. Here we demonstrate a microfluidic device that integrates live slice cultures with an intuitive multiwell platform that allows for exposing the slices to multiple compounds at once or in sequence. We demonstrate the response of live mouse brain slices to a range of drug doses in parallel. Drug response is measured by imaging of markers for cell apoptosis and for cell death. The platform has the potential to allow for identifying the subset of therapies of greatest potential value to individual patients, on a timescale rapid enough to guide therapeutic decision-making.

<sup>a</sup> Department of Bioengineering, University of Washington, Seattle, WA, USA. E-mail: [afolch@u.washington.edu](mailto:afolch@u.washington.edu); Fax: +1 206-543-6124; Tel: +1 206-685-2257

<sup>b</sup> Department of Neurosurgery, University of Washington, Seattle, WA, USA.

<sup>c</sup> Department of Pathology and Genome Sciences, University of Washington, Seattle, WA, USA.

\* Corresponding author

Electronic Supplementary Information (ESI) available: [details of any supplementary information available should be included here]. See DOI: 10.1039/b000000x/

### Introduction

The National Cancer Institute has identified that "current methods to assess potential cancer treatments are cumbersome, expensive, and often inaccurate" and has issued the challenge "to develop methods to rapidly test interventions for cancer treatment or prevention"<sup>1</sup>. This need is pertinent even in the more severe cases of malignant tumors. For example, malignant gliomas constitute about 80% of the primary malignant tumors in the central nervous system and are essentially incurable<sup>2</sup>. Patients diagnosed with glioblastoma multiforme (GBM), which comprise over two-thirds of all adult malignant primary brain tumors, have a median survival of about one year and overall 5-year survival rate of <5%. Despite advances in surgical technique, delivery of chemotherapy and radiation<sup>2</sup> and myriad clinical trials, the dismal outcomes for GBM patients has not improved significantly in the last four decades. This grim reality reflects the marginal effectiveness of current treatments that are applied to cancer patients without consideration of the enormous impact of inter-individual variations in

tumor phenotypes<sup>3,4</sup>. The advent of high-throughput genomic profiling and drug screening techniques heralds a new era of targeted cancer therapy, in which the identification of patient-specific cancer biology and drug response profiles can be used to inform therapy. As noted by NCI, significant challenges remain in developing more robust and practical pre-clinical drug screening techniques.

The most commonly proposed screening methods for malignant tumors utilize isolated tumor cell cultures or patient-derived xenografts (PDXs). However, cultured tumor cells disrupt interactions with the tumor microenvironment and may not retain phenotypic heterogeneity of tumor cells in situ, both critical factors in treatment response and resistance<sup>5,6</sup>. In contrast, while PDX models retain phenotypic heterogeneity and tumor microenvironment features, they are cumbersome, expensive, and typically take weeks to months to establish and expand. Therefore, PDX models cannot provide drug response data before the therapy is initiated (2-3 weeks) after surgery. Thus, PDXs are impractical for guiding patient-specific decision-making.

Co-culture and three-dimensional (3D) cell culture environment tend to recreate behaviors which are physiologically relevant to live tissues. As tumor cells co-exist with other types of cells and grow in a 3D environment, both culture methods can better recapitulate the tumor physiology than traditional 2D cell cultures<sup>7,8</sup>. These improved cell culture models have accelerated the discovery of tumor-stromal, ECM interactions and cell-to-cell signaling led to the realization of the complexity of the tumor microenvironment<sup>9</sup>. However, these models are technically challenging and are normally created based on

simplified assumptions of tumor physiology, rather than created from individual patients' tumor tissue.

Therefore, there is an urgent need to develop approaches to rapidly and reliably assess the response of intact primary tumor specimens to a range of possible therapies, with the goal of identifying the most effective subset of therapies for individual tumors and patients. A relatively unexplored, alternative system for patient-specific drug sensitivity profiling, patient-derived "organotypic" slice cultures (PDSCs), addresses many of these challenges. Compared to cell cultures, PDSCs retain both tumor cell heterogeneity and tumor microenvironment. In contrast to PDXs, PDSCs can be tested to provide drug response data before the therapy is initiated. Unlike co-culture and 3D culture, PDSCs require simple techniques and allow for preservation of original tumor specimens from individual patients. As evidence mounts that the surrounding stromal cells play a key role in tumorigenesis and tumor progression<sup>10</sup>, increasing numbers of cancer groups have been utilizing tumor tissue slice approaches that may better replicate tumor physiology for pharmacodynamic and cancer biology studies. Many laboratories have adopted the "organotypic" tissue culture technique<sup>11</sup> (i.e., on porous membrane supports) with great success<sup>12-16</sup>. For example, Massimo Loda's group recently showed that the PI3K/Akt signaling pathway (whose activity is affected by epithelial-stromal interactions) could be inhibited in lung and colon tumors, resulting in a partial decrease in tissue proliferation and viability<sup>14</sup>; the results were reproduced with other tumors and inhibitors, demonstrating that it is possible to test the effects of therapeutic agents in viable tumor tissue with preserved microenvironments. In most studies with organotypic culture, drug is uniformly applied to the slice. As the number of tumor slices is limited, this approach dramatically limits the numbers of conditions that can be tested.

Unfortunately, unlike cell cultures, PDSCs lack a standardized high-throughput drug delivery system. Microfluidic devices have shown the potential for delivering reagents locally to an intact tissue slice<sup>17,18</sup>. However, the difficulty in device operation and low throughputs (one drug application per slice) make such devices unappealing for clinical use. To improve these shortcomings, we have developed a user-friendly microfluidic device that permits regioselective delivery of large numbers of drugs with spatiotemporal control in slice cultures.

## Materials and methods

### Fabrication of a 96-well plate-based microfluidic device

A 96-well plate-based microfluidic device was fabricated using soft-lithography, poly(dimethylsiloxane) (PDMS) replicas, oxygen plasma for PDMS-PDMS and PDMS-glass bonding, and silane coupling for PDMS bonding. The device was assembled from 4 parts including a modified bottomless 96-well plate, a PDMS layer containing through holes, a PDMS channel network layer, and a thin microfluidic chip.

The bottomless 96-well plate is modified to fit a square reservoir in the center of the plate by sacrificing a 4x4 well area, thus the device only accepts 80 inputs instead of 96. The PDMS through-hole layer

contains 3-mm holes and a central square which were done by exclusion molding from a laser-cut rectangular mold to create a uniform rectangular PDMS block, followed by punching 3-mm holes and cutting the central square to match the modified 96 well plate. The PDMS channel network layer consists of two separate PDMS molds to assemble a complete channel network to distribute the fluids from the well inlets to the tissue. The microfluidic chip has 80 parallel open channels which sit beneath a PTFE porous membrane. Each open channel is 8 mm in length and 100  $\mu\text{m}$  in width. The flow rates of all channels are equilibrated by adjusting the microchannel resistances (i.e. changing their widths according to their lengths). Detailed fabrication protocols are described in Supplementary notes.

### Organotypic slice culture in a microfluidic device using a PTFE membrane transfer technique

Hydrophilic polytetrafluoroethylene (PTFE) porous membranes are a standard material for organotypic slice culture<sup>19,20</sup>. PTFE has a mesh-like topography and fibrous structure with high permeability and porosity, which help transport nutrients across the whole surface of the slice. Other porous membrane materials (e.g. track-etched polyethylene terephthalate (PET) or polycarbonate (PC) membranes) that we tested resulted in poor slice viability compared to PTFE membranes (Supplementary Fig. 2). Here we demonstrate an easy method to transfer the PTFE membrane (with attached mouse brain slices) on top of the open microchannels, which closes the roof of the microchannels. This transfer can be easily done by cutting the membrane from the PTFE membrane well insert with the tissue slice cultured on the top and then placing it in the device (the PTFE porous membrane must fully cover the open channels). This method relies on the paper-like (wicking) properties of the PTFE material which has a very low surface tension; even when the PTFE is moist, the PTFE establishes an excellent seal with a PDMS substrate. We observe that the fluidic streams penetrate the membrane, causing transport of solutes to slices in a spatially-defined manner.

After drug exposure, the membrane and tissue slice can be removed from the device for washing, staining, and imaging. Since the tissue only contacts the membrane, the multi-well plate platform can be washed and reused with new membrane and tissue slices. Our membrane transfer technique thus enables slice culture, drug exposure, and post-exposure tissue processing to be done in three physically separable steps without damaging the integrity or viability of the tissue (Supplementary Fig. 3).

### Organotypic mouse brain slice culture

Coronal mouse brain slices were prepared from E18~P7 embryonic or neonatal mice supplied by Charles Rivers Laboratories. Pregnant or neonatal mice were sacrificed in accordance with a protocol approved by the University of Washington Animal Care and Use Committee. Brain slices were prepared in ice-cold, Gey's balanced salt solution (GBSS; #G9779, Sigma, St. Louis, MO) supplemented with glucose (D-Glucose; G-6152, Sigma, St. Louis, MO) to a concentration of 7.5 mg/mL and bubbled with carbogen (5% CO<sub>2</sub> and 95% O<sub>2</sub>) under sterile conditions. Mice were sacrificed by decapitation, and the brain removed and quickly immersed in ice-cold, carbogen bubbled artificial cerebrospinal fluid (ACSF) prior to vibratome slicing

(Vibratome Series 1000, Technical Products International, St. Louis, MO). The cerebellum and inferior colliculus were removed with dissection scissors to create a flat tissue surface to allow vibratome stage mounting prior to slicing. A 6% rectangular agarose block was mounted on the vibratome stage using superglue as a wall for the whole mouse brain. Once the whole mouse brain was on the stage, ice-cold carbogen bubbled ACSF was quickly transferred into the vibratome stage to immerse the whole brain. Crushed ice was used to surround the vibratome stage to maintain temperature during slicing with an uncoated razor (American Safety Razor Company, Verona, VA) to produce 300  $\mu\text{m}$  thick brain slices. Brain slices were transferred onto PTFE membrane culture inserts (PICM0RG50, Millipore, Billerica, MA) using a 3-mm plastic transfer pipet (#357575, BD Bioscience, San Jose, CA) with the tip removed. Culture inserts were prepared and placed in a 6-well plate containing pre-warmed culture medium (1.2 ml medium/well/insert). The culture medium contained 75% Neurobasal-A (#10888, Invitrogen, Carlsbad, CA), 25% horse serum (#H1138, Sigma-Aldrich, St. Louis, MO), Penicillin-Streptomycin (#P0781, Sigma-Aldrich, St. Louis, MO) and L-Glutamine (#G7513, Sigma-Aldrich, St. Louis, MO). Once positioned on the PTFE membrane the surrounding solution (ACSF) was removed to create an air-fluid interface. The slices were then cultured in a tissue culture incubator with medium replacement every two days.

Here we used mouse brain slices to demonstrate our microfluidic platform because organotypic slice cultures are well-established in neuroscience research<sup>21</sup> and have been used with great success and consistency by many groups<sup>20,22-24</sup>. We were able to confirm high viability of brain slices in our device after 2 and 7 days in culture using vital staining dyes prior to starting dose-dependent toxicity studies (Supplementary Fig. 4).

#### Human GBM xenograft mouse brain slice culture

The human glioblastoma cell line GBM8 was used in the current study<sup>25</sup>. The cells were characterized for invasive and migratory behaviors both *in vitro* and *in vivo* and then confirmed for positive response to Temozolomide (TMZ)<sup>25</sup>. GBM8 cells were labeled by lentiviral GFP expression to allow for the identification of the cells prior to xenograft generation. Xenografts were generated by injecting 200,000 viable glioma cells (trypan blue, a dead cell-selective dye, was used to determine the viability of cells) orthotopically into immunodeficient nude mice as described<sup>26</sup>, grown *in vivo* for ~4 weeks to allow tumor formation. The preparation and generation of the GBM xenograft slices followed the same protocol as mouse brain slices, except they were 400  $\mu\text{m}$  thick. GBM xenograft slice cultures were performed in culture medium supplemented with epidermal growth factor (EGF; 20 ng/mL; #PHG0311 Invitrogen, Carlsbad, CA) and fibroblast growth factor (FGF; 20ng/mL; #PHG0264 Invitrogen, Carlsbad, CA). Xenograft slices were transferred to PTFE membrane well inserts for culture. The resulting GBM xenograft slices contained glioma cells spreading out in the mouse brain from the original injection site with a characteristic architecture (Supplementary Fig. 5).

#### Device operation for drug screening

The assembled microfluidic device was treated with oxygen plasma using the same conditions for bonding, sterilization and hydrophilization prior to use. Immediately after the plasma treatment, the device was transferred to a cell culture hood and microchannels were filled by pipetting culture medium into well reservoirs, covering the open channels with a PTFE membrane and then applying suction to the outlet. Once microchannels were filled, the device was left in a cell culture incubator for 1 hr to allow culture medium to temperature and pH equilibrate prior to use. Tissue slices were transferred from the porous membrane well insert by first cutting PTFE membrane and placing it onto the open microchannels of the device. The full culture area of the device (80 parallel open channels) was imaged to register the position of tissue slices relative to delivery channels. Well reservoirs were then filled with either drug or buffer with the desired spacing (~2-4 buffer channels in between each of two delivery channels). Drug channels contained staurosporine (STS; #S6942, Sigma-Aldrich, St. Louis, MO) or TMZ (#T2577, Sigma-Aldrich, St. Louis, MO) to induce cell killing in mouse or human GBM mouse xenograft slices, respectively. Flow was initiated by connecting the device outlet to a 20 ml syringe (#302830, BD Bioscience, San Jose, CA) and syringe pump (Fusion 200, Chemyx Inc., Stafford, TX) to ensure a flow rate of 300~1200  $\mu\text{L}$  per hour.

#### Live-tissue staining and post-tissue processing

LIVE/DEAD cell staining (Invitrogen, Carlsbad, CA) was used to detect dead cells stained with red-fluorescent ethidium homodimer-1 (EthD-1), and live cells stained with green fluorescent calcein-AM, in mouse brain slices. Brain slice was rinsed 3 times with PBS, then submerged in 4  $\mu\text{M}$  calcein-AM and 2  $\mu\text{M}$  EthD-1 mixed solution at room temperature for 1 hr followed by three PBS rinses before imaging. We found that mouse brain slices should be cultured for at least 3 days to reach peak viability and recover from cell damage caused by tissue preparation.

CellEvent™ Caspase-3/7 Green Detection Reagent (#C10423, Invitrogen, Carlsbad, CA) and Fixable Viability Dye eFluor 660 (eBioscience, San Diego, CA) were used to detect cell apoptosis and cell death respectively. DAPI (#D3571, Invitrogen, Carlsbad, CA) was used to label cell nuclei. After drug exposure, mouse brain slices were removed from the device and submerged in 1  $\mu\text{M}$  CellEvent™ and 1  $\mu\text{M}$  Fixable Viability Dye eFluor 660 mixing solution in PBS at room temperature for 1 hr, followed by fixation in 4% PFA at 4 °C overnight. Tissue slices were then permeabilized with 0.1 % Triton X-100 (#T8787, Sigma-Aldrich, St. Louis, MO) for 30 min following by 100nM DAPI staining overnight. Tissue slices were then rinsed 3 times with PBS (5 min/cycle) prior to clearing by immersion in ScaleView A2<sup>27</sup> (Olympus, Center Valley, PA ) for at least 2 d prior to imaging.

#### Image acquisition

Tissue slices were imaged in a glass-coverslip bottom chamber (#12565336, Fisher Scientific, Pittsburgh, PA) using a Nikon Eclipse Ti inverted microscope (Nikon Instruments, Melville, NY) with epifluorescence illumination. An automated x-y stage and both 4X and 10X objectives were used to acquire fluorescent images. Images with 10% overlap were subsequently stitched together to generate

fluorescence images. Individual images were focused manually during stitching. All the images were acquired with a 12-bit cooled CCD camera (ORCA-ER, Hamamatsu, Japan). Nikon NIS-Elements AR software was used to control image acquisition.

Confocal images were obtained using a Zeiss LSM 510 confocal microscope (Carl Zeiss, Thornwood, NY) with a 20X objective. Drug-treated and control regions were located visually using the binoculars of the microscope. The thickness of optical sections was 2.2  $\mu\text{m}$ , based on the longest excitation wavelength of the fluorescent channel. All three fluorescent channels were set to the same optical thickness. The z-scan function was used to define the surface (0  $\mu\text{m}$ ) of the tissue slice, then confocal image acquisition started 10  $\mu\text{m}$  above the bottom tissue surface (which was in contact with the PTFE membrane sealing microchannels). Five optical slices (~2.2  $\mu\text{m}$  thick/optical section) separated by 10  $\mu\text{m}$  and 50  $\mu\text{m}$  deep in tissue slices were acquired from both STS-treated and buffer control regions. The maximum optical depth of 50  $\mu\text{m}$  was selected to ensure high overall fluorescence intensity. Confocal images were then acquired sequentially in tissue slices at the regions of interest.

#### Image processing and data analysis

ImageJ was used to convert epifluorescence images into two-dimensional fluorescence intensity plots for brain regions of interest. In our experiment, the dorsal cortex area of mouse brain slices in epifluorescence images was manually selected. The fluorescence intensities (y-coordinate) at a particular distance along the slice (x-coordinate) is obtained by averaging the pixel intensities from the selected dorsal cortex region (yellow-dashed regions in Fig. 3a and 3c), and normalizing with respect to the maximum average intensity measured. The measurement of the normalized fluorescence intensities from plots could then be used directly to gauge drug and dose-dependent responses in tissue slices from the region(s) of interest.

ImageJ with an automatic nuclei counter plug-in was used to convert confocal images into cell counts (Supplementary Fig. 6). We used inputs of 14 pixels for the diameter of a cell and 7 pixels for the minimum distance between cells to analyze all the confocal images. An additional parameter, threshold, was set at 1 for DAPI and apoptotic cells, and at 2 for dead cells to improve counting accuracy. Captured images were opened in ImageJ to quantify and report positive cell staining in fluorescence images as cell counts that were exported to an Excel spreadsheet for further analysis. The combination of cell counts (DAPI, apoptotic cells, and dead cells) was quantified by calculating percentages of cell apoptosis and cell death from each image captured in spreadsheet data.

#### Comsol modeling of 2D diffusion-based concentration profiles in tissue slices

Using Comsol's Free and Porous Media Flow module, we approximate the porous matrix properties of brain tissue slices with a constant porosity of 0.4, a permeability of  $1.0 \times 10^{-11} \text{ m}^2$ , and a tortuosity of 1.5<sup>28</sup>. The Transport of Diluted Species module was used to define the concentration sources and sinks at the selected microchannels with STS (M.W. = 466 Da) as the

diffusing species (diffusion coefficient ( $D$ ) =  $5.7 \times 10^{-10} \text{ m}^2\text{s}^{-1}$ ) to simulate concentration profiles in tissue slices.

## Results and discussion

### Microfluidic device design

Here we demonstrate a microfluidic platform that allows for selective delivery of fluids to an organotypic slice at a large number of pre-defined locations. Delivery of drugs occurs through a removable porous membrane that rests on top of a set of microchannels. Each microchannel is fed by a 400  $\mu\text{L}$  reservoir that, given the low flow rates (~7.5  $\mu\text{L/hr}$  per microchannel) can provide up to ~48 hrs of uninterrupted reagent delivery. After reagent delivery, the membrane (with slice attached) can be removed for imaging and analysis.

The platform features a "tubeless" input interface based on 96-well format (inspired by work from Brian Cunningham's group<sup>29</sup>). The central 4x4 wells from the 96-well plate have been removed by means of a laser cutter (Universal Laser Systems, Scottsdale, AZ) to create a culture area, while the remaining 80 wells serve as reservoirs (inputs) in our device (Fig. 1a). As opposed to other interfaces based on tubing and connectors, this familiar, user-friendly interface allows users to pipet panels of up to 80 solutions into the device. With this microfluidic organotypic culture, solutions move through channels on the bottom surface and then travel or diffuse upwards through the tissue (the porous membrane is in contact with solutions to ensure proper wetting of the membrane and the tissue).

Our microfluidic device for slice cultures was fabricated by using a combination of multilayer soft lithography, exclusion molding<sup>30</sup> and PDMS-to-plastic silane bonding<sup>31</sup>. Upstream of the delivery/culture area, each microchannel is individually connected to a different reservoir well of the modified 96-well plate, containing a drug of choice (Fig. 1b). Downstream of the delivery area, all the microchannels are connected to a common outlet via a binary arbor; we typically control flow with a syringe pump, but it is also possible to run flow by gravity to a lower common reservoir (siphon) (Supplementary Fig. 7). The delivery microchannels, initially "roofless", are separated by PDMS walls. The PDMS walls are designed to sit underneath a PTFE porous membrane. When a wet PTFE porous membrane is placed onto the open microchannels, capillary forces cause the membrane to adhere to the PDMS surface; the membrane then becomes the "roof" for the open microchannels. Negative pressure applied to the outlet increases the PTFE membrane adhesion to the PDMS surface and causes a slow flow under the membrane, allowing for the diffusive supply of nutrients to the tissue. All the microchannel resistances (and thus flow rates) are designed to be equivalent across all microchannels, which were achieved by varying microchannel widths according to their lengths.

All the PDMS and plastic components in the 96-well plate-based device (except the porous membrane) are irreversibly bonded to produce a leak-proof platform (Fig. 1c-d). This 96-well plate platform results in a device that is easy to transport, and is compatible with standard imaging systems.

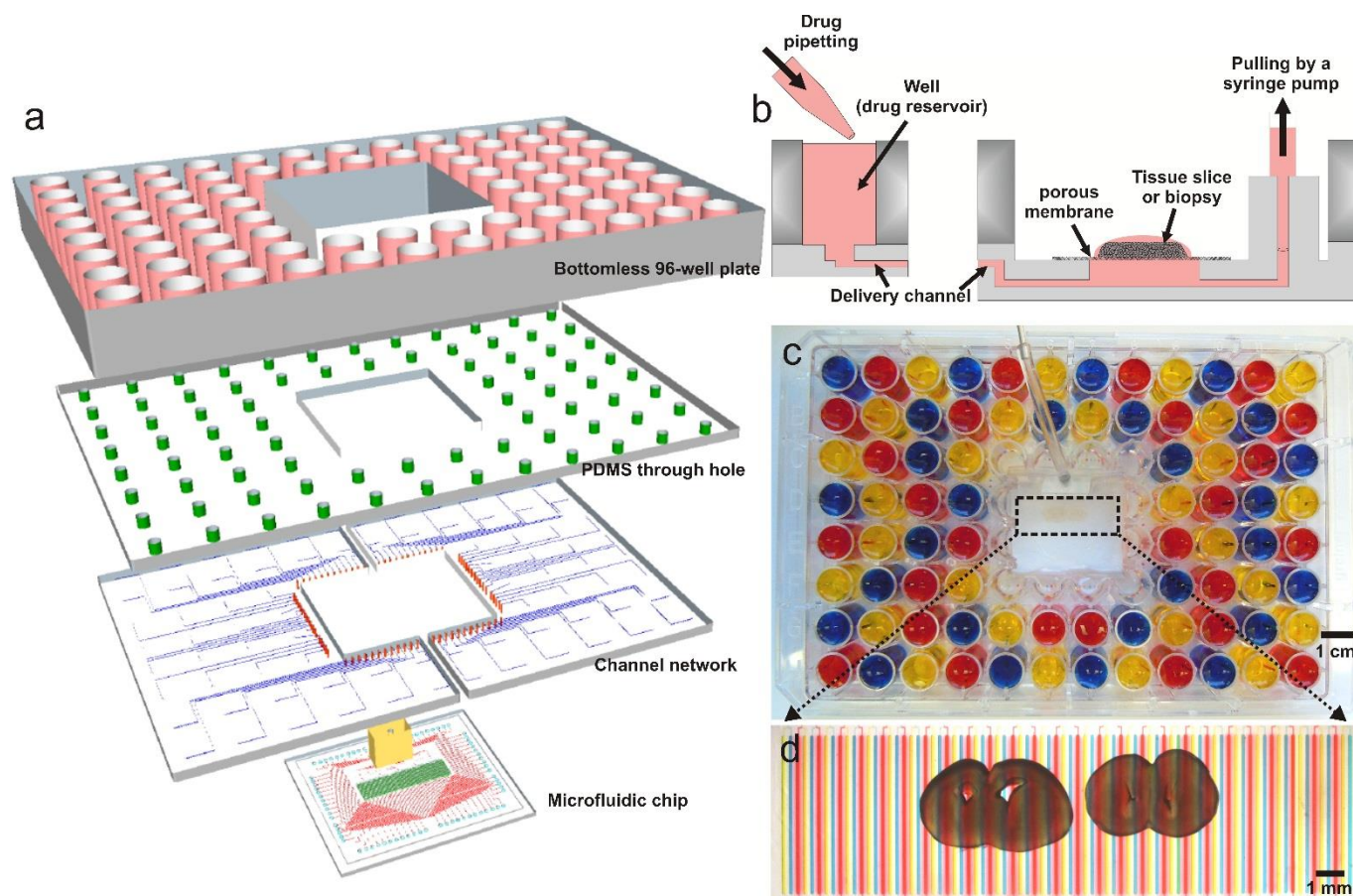


**Figure 1.** Microfluidic device design (a) Layer-by-layer schematic view of the device. The device includes (from top to bottom) a modified bottomless 96-well plate featuring 80 inlet wells after the central 16 wells have been removed; a PDMS layer containing through holes layer; a PDMS microchannel network layer; and the microfluidic chip (where the porous membrane with the tissue is placed). (b) Cross-sectional schematic of the device. The device is operated by gravity flow and the total flow rate is driven by a syringe pump through a common outlet: one syringe pump is able to control flow across all 80 fluidic streams. Tissue slices are cultured on a PTFE porous membrane. The wet membrane seals the open microchannels by capillarity, which allows for fluidic stream transport of culture medium to tissue. (c) Micrograph of the microfluidic platform loaded with three dyes (yellow, blue and red) in sequence to generate an alternating pattern of yellow, blue and red microchannels across the perfusion membrane. (d) Micrograph of the tissue culture area after loading the platform shown in (c) with a porous membrane that has two mouse brain slices attached.

### Selective mass transport into an intact tissue

To explain transport in our microfluidic device, we consider the PTFE porous membrane separate from the tissue slice. In theory, the membrane's mesh structure creates high hydrodynamic resistance: therefore, the porosity of the membrane allows molecules to diffuse into the membrane without convection. We tested the fluid transport within a PTFE porous membrane placed in our microfluidic device using fluorescein (M.W. 332 Da). We observed that lateral diffusion of reagents within the membrane can be adjusted by varying the flow velocity of the fluids in the microchannels underneath the membrane (Fig. 2a). From this observation, we felt the need to evaluate whether the membrane can support flow when the latter is driven by the fluid streams in the microchannels.

In order to investigate this fluid transport phenomenon, we used fluorescently labelled dextran with different molecular weights (M.W. 3000 and 70,000) to determine if the fluid transport is dominated by convection or by diffusion. We found that the spreading length of fluorescence signal is altered by different M.W. (Supplementary Fig. 8a-b), which indicates that the dominant mode of transport within the membrane is by diffusion. Furthermore, we performed an additional

experiment using quantum dots (5–20 nm in diameter) (Supplementary Fig. 8c). No single quantum dot was observed outside of the channel region, indicating that the flow lines from the fluid streams in the microchannels do not significantly penetrate the PTFE porous membrane.

To further understand how our microfluidic device can achieve selective drug delivery to a tissue slice, we built a simple diffusion-based model using Comsol. In our microfluidic device, the drug delivery channels (containing concentration  $C_1$ ) are separated by buffer channels (concentration  $C_0$ ). In the Comsol model, we assumed delivery and buffer channels in direct contact with a 200  $\mu\text{m}$  thick 2D “tissue slice” (Fig. 2b) which is assumed to be a homogeneous porous medium<sup>28</sup>. Comsol simulations that use configurations of delivery and buffer channels different from that in Fig. 2b are shown in Supplementary Fig. 9. The delivery channels act as concentration sources which isotropically diffuse into tissue slices. Buffer channels next to delivery channels act as concentration sinks that limit diffusion from delivery channels. Hence, the flows in both delivery and buffer channels create stable sources and sinks that result in the formation of steady-state chemical concentration patterns over time inside tissue

slices (Fig. 2b). The concentration plot in Fig. 2b shows the predicted concentration profiles at 10  $\mu\text{m}$ , 25  $\mu\text{m}$ , 50  $\mu\text{m}$ , and 100  $\mu\text{m}$  above delivery channels in a tissue slice.

We have been able to visualize these predicted concentration patterns in tissue slices by using fluorescent cell tracers. We delivered two different colors of cell nuclear staining reagents, Hoechst (blue) and Sytox Green (green) to a fixed mouse slice (Sytox Green can

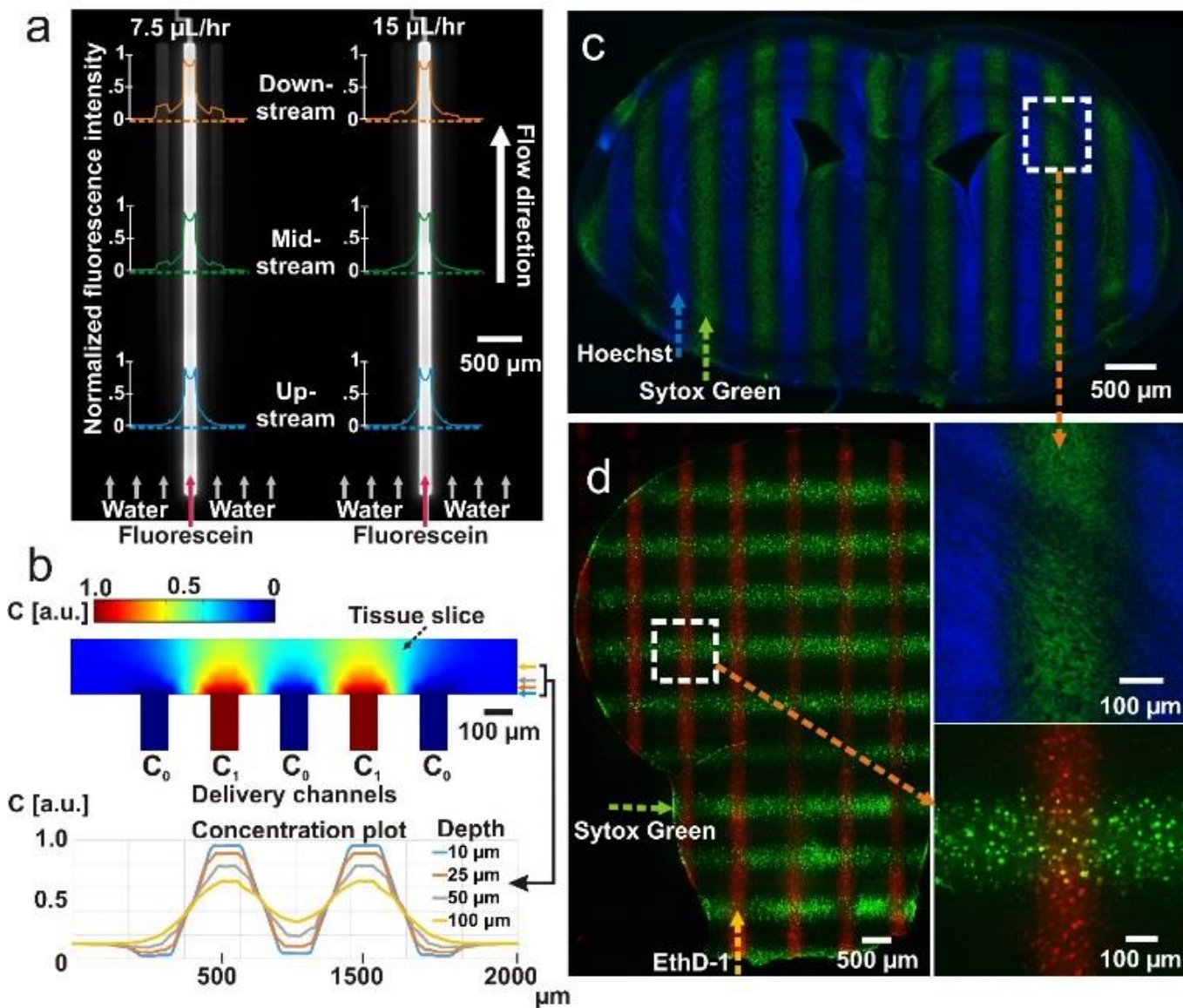


**Figure 2.** Selective chemical delivery to tissue slices. (a) Transfer from the underlying fluid streams into the PTFE porous membrane: the extent of lateral diffusion within the membrane (direction orthogonal to flow) scales with the flow velocity underneath the membrane, as one would expect from a free-flowing laminar flow. (b) Steady-state concentration profile modeled with Comsol using an ideal 200  $\mu\text{m}$ -thick tissue slice under conditions of diffusion-based transport. The drug ( $C_1$ ) and buffer ( $C_0$ ) channels act as infinite sources and sinks, respectively. (c) Micrograph of a fixed mouse brain slice exposed to two different cell nuclear binding agents (Hoechst, blue, and Sytox Green, green) through the alternating streams in our microfluidic device for 5 hrs. The image is the result of stitching 42 fluorescence microscopy images. (d) Demonstration of sequential drug exposure. The porous membrane is rotated and repositioned (with tissue attached to the membrane) in the device between the first and the second reagent deliveries. As a result,  $n$  reagents delivered in parallel result in the formation of  $n^2$  junctions where  $n^2$  sequential pairs of reagents (“sequences”) are delivered. For this sample, the image only contains half of a mouse brain slice because the width of a coronal-cut adult mouse brain slice is longer than the fluidic channels.

This simple diffusional model neglects the contribution of advection (mass transport due to fluid’s bulk motion) potentially caused by injected flow at the bottom slice surface into the porous tissue and/or by evaporation of fluid at the top slice surface. In both cases, fluid momentum would be directed upward, and would enhance patterned delivery. Thus our model provides a lower estimate of the observed spatial drug distribution profiles.

only enter into cells with compromised cell membranes) for 5 hrs through alternating streams using our microfluidic device. These staining reagents can be selectively delivered to the regions of the tissue slice with minimum lateral diffusion between the delivery channels, as shown in Fig. 2c. To measure the penetration depth of reagents into the tissue slice, we have conducted confocal studies of Hoechst dye penetration in a live mouse brain slice, showing at least 50- $\mu\text{m}$  penetration in 1 hour of Hoechst dye (Supplementary Fig. 10).

A recent report from Yaffe's group has discovered that delivering inhibitors that target oncogenic signaling pathways to a subset of triple-negative breast cancer cells prior to treating with chemotherapeutic agents such as doxorubicin increased the sensitivity of cancer cells to killing by genotoxic drugs<sup>32</sup>. This sequential treatment suggests a potential approach to activate oncogenic signaling pathways, rendering tumor cells more susceptible to chemotherapeutic drugs before chemotherapy. In order to demonstrate the ability of our platform to perform sequential exposures in orthogonal format for a future sequential assay, we performed two consecutive deliveries of fluorescent tracers, EthD-1 (red) and Sytox Green (green), to a fixed mouse brain slice by rotating the porous membrane at 90 degrees in between the first and the second reagent delivery (Fig. 2d and Supplementary Fig. 11). The drug reservoirs after the first reagent delivery are rinsed thoroughly before the slice is rotated. This technique potentially allows for the delivery of  $n$  delivered drugs and  $n^2$  combinations to the junctions.

### Measurement of chemosensitivity profiles in an intact mouse brain slice

In order to test the ability of our microfluidic platform to produce dose-dependent chemosensitivity profiles of an intact tissue, we used STS, a non-selective alkaloid protein kinase inhibitor, on mouse brain slices. STS mimics the application of chemotherapeutic drugs to intact tumor tissue slices by inducing apoptosis<sup>33,34</sup>. After STS drug delivery, the mouse brain slices were stained with CellEvent™ Caspase-3/7 Green Detection Reagent, which detects apoptotic cells. CellEvent™ is compatible with both live cell fluorescence-imaging and paraformaldehyde (PFA)-based fixation methods. Therefore, after staining and prior to imaging, the brain slices were fixed using 4% PFA. An epifluorescence microscope with an automated stage was used to capture the image of whole mouse brain slices.

We first delivered the same dose of STS in culture medium containing 1  $\mu\text{M}$  of STS for 18 hrs, with an interval of four buffer channels in between each of two STS delivery channels to an intact mouse brain slice. We observed significant apoptosis (cells labeled with CellEvent™) at the STS-treated regions (Fig. 3a) after 18 hrs of STS delivery. In order to quantify the fluorescence intensity from the epifluorescence image (Fig. 3a), we selected the dorsal cortex region from the image of the mouse brain slice (yellow-dashed region in Fig. 3a). The dorsal region has a relatively uniform cell density, which allowed us to establish a fluorescence intensity readout of cell apoptosis across STS-treated regions more easily than in other regions with more variable cell density or tissue porosity. Similar fluorescence intensity profiles across four STS-treated dorsal brain regions was observed as shown in Fig. 3b (the standard error of the mean, averaged over the 100  $\mu\text{m}$  wide drug delivery channels, was 7.1% and mostly attributable to the rightmost data peak). This result not only shows the feasibility of quantifying readouts based on epifluorescence images, but also demonstrates the reproducibility of outcomes from different drug-treated regions with the same dose of drug exposure.

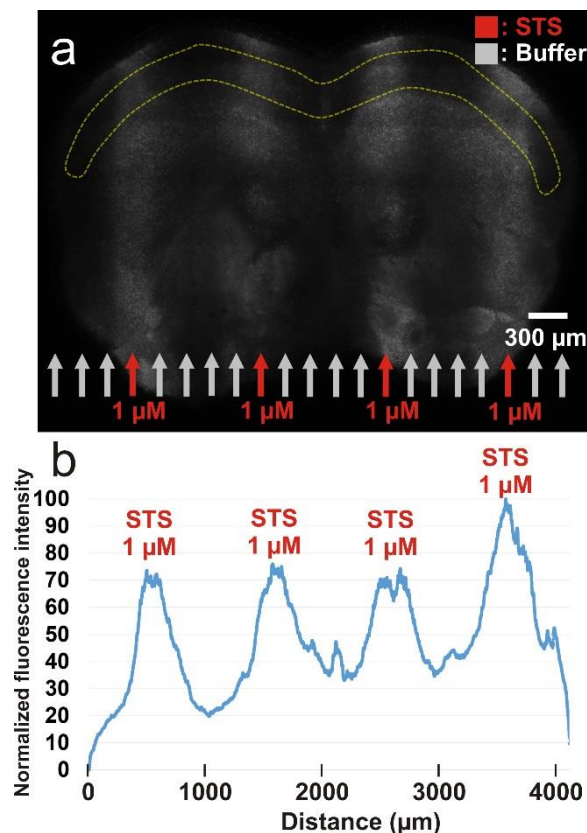


**Figure 3. Drug response in intact mouse brain slices.** STS was used as a model cytotoxic agent. (a) Equivalent doses (1  $\mu\text{M}$  for 18 hrs) of STS were delivered to coronal-cut mouse brain slices with the same interval distance (four buffer channels) in between each of two STS solutions. Fluorescent lanes indicate apoptotic cell staining by CellEvent™ in STS-exposed regions. (b) 2D fluorescence intensity profile across dorsal cortex of the mouse brain slice (yellow dashed region in panel a). The plot shows peaks of fluorescence intensity across STS-exposure areas.

Next, different doses of STS drug solution (culture medium containing 6  $\mu\text{M}$ , 4  $\mu\text{M}$ , 2  $\mu\text{M}$ , 1  $\mu\text{M}$ , 500 nM, 100 nM, 10 nM of STS) were delivered to an intact mouse brain slice with a separation of two buffer channels in between every two STS delivery channels (Fig. 4a). Note that we consider the process of loading different concentrations of STS is similar to loading different drug compounds. The slice was exposed to the STS solution at the selected regions for approximately 8 hrs to allow induction of apoptosis. The resulting images show that apoptotic cells stained by CellEvent™ (bright cell nuclei) form lines over channels used to deliver STS, and that fluorescence intensity from labelled cells increased with the dose of STS (Fig. 4a). Our results demonstrate that the intensity profile measured from the dorsal cortex area increases in an STS dose-dependent manner (Fig. 4b). A diffusion-only Comsol model that simulates the delivery of STS as in Fig. 3 (1  $\mu\text{M}$  for 18 hrs) and Fig. 4 (6  $\mu\text{M}$ , 4  $\mu\text{M}$ , 2  $\mu\text{M}$ , 1  $\mu\text{M}$ , 500 nM, 100 nM, 10 nM for 8 hrs) produces concentration profiles shown in Supplementary Fig. 12. The fluorescence intensity plot (Fig. 4b) from our experimental study and the simulated concentration plot (Supplementary Fig. 12b) obtained from Comsol modeling show a strong correlation ( $R^2 = 0.933$ ), indicating that the fluorescence intensity readouts generated using the apoptotic marker (averaged over the 100  $\mu\text{m}$ -wide drug delivery channels) are significantly correlated with STS concentration.

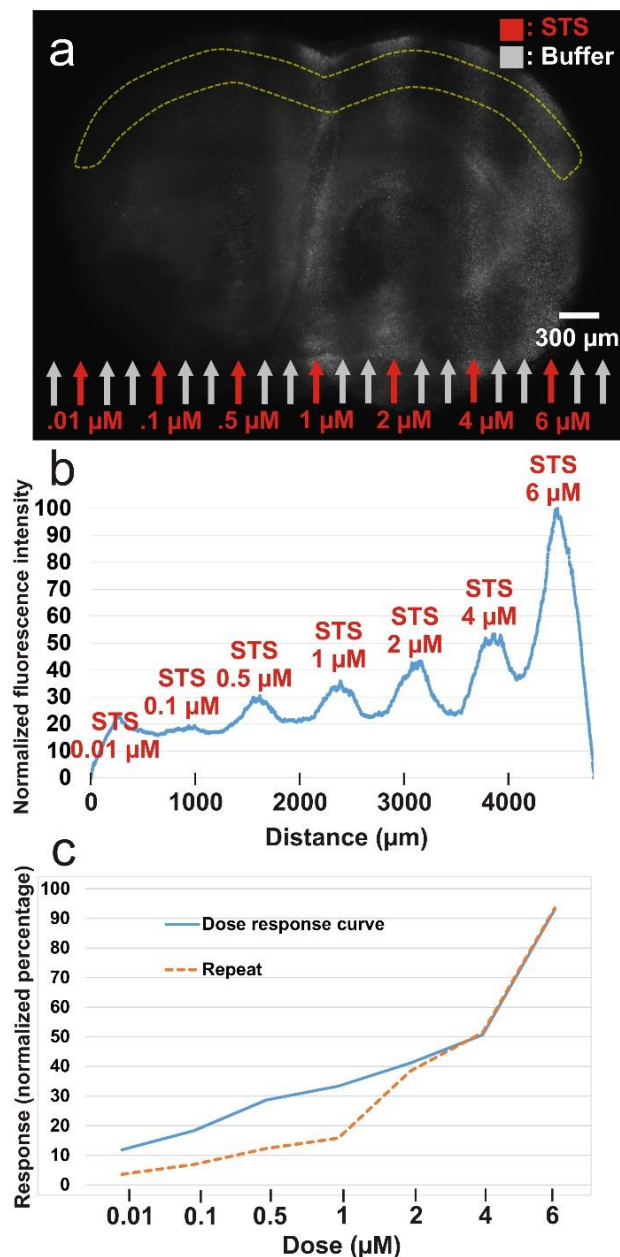


**Figure 4. Dose-dependent cytotoxicity in intact mouse brain slices.** STS was used as a model cytotoxic agent. (a) Different doses of STS solution were delivered to a coronal-cut mouse brain slice with the same interval distance (two buffer channels) in between each of two STS solutions. Fluorescent lanes of apoptotic cells stained by CellEvent™, formed at the STS-exposed regions in which the density of apoptotic cells is positively correlated with the STS dose. (b) 2D fluorescence intensity profile across dorsal cortex of the mouse brain slice (yellow dashed region in panel (a)). The plot shows that the peaks of the fluorescence intensity located at the STS exposure areas correspond with the doses of STS in a dose-dependent manner. The fluorescence intensity plot can be directly used as a drug screening readout on intact tissues. (c) Concentration plot of the dose-dependent experiment. The orange dash curve is a repeat.

Further, a dose-response plot quantified by averaging the response values over the drug delivery channels is shown in Fig. 4c. A repeated experiment (orange dash line in Fig. 4c) shows a similar concentration plot with a strong correlation ( $R^2 > 0.95$ ).

#### Optical slices for data quantification

Epifluorescence images of apoptotic cells (as shown in Fig. 3a, 4a and 5a) allow for fluorescence intensity, but may not directly reflect the number of labeled cells due to variations in drug/stain penetration, optical focus, light absorption, or labeling efficiency. Confocal or multi-photon microscopy can address these issues by using thin optical sections to visualize individual cells labeled with intracellular reagents. The numbers of individually labeled cells can then be counted using automated cell counting software (e.g. Image J) to provide a more accurate estimate of the number and proportion of dead cells over a perfusion channel.

In order to demonstrate the ability of confocal imaging to collect quantitative cell function data from intact perfused tissue slices, we compared STS-treated (culture medium with 1  $\mu\text{M}$  STS) and buffer regions (culture medium alone) to detect cell nuclei by DAPI staining together with apoptotic and dead cells (Fig. 5b-c). The cell counts of apoptotic cells and dead cells from each confocal image are expressed as percentages with respect to total cells. Each bar represents the average percentage of 5 confocal images (depth in the tissue: 0  $\mu\text{m}$ , 10  $\mu\text{m}$ , 20  $\mu\text{m}$ , 30  $\mu\text{m}$ , 40  $\mu\text{m}$ ) at that specific region (Fig. 5d-e). Our results show that the percentages of cell apoptosis and cell death were on average 7.4-fold and 6.8-fold higher, respectively, at the STS-treated regions than at the buffer regions (Fig. 5d-e). These results are statistically significant with the p-value  $< 0.001$  using student t-test (two-sample assuming equal variances), and provide more detailed information than is contained in epifluorescence images (Fig. 5a). We directly compare the average percentages of the apoptotic cells (Fig. 5f) and dead cells (Fig. 5g) between the STS-treated and buffer regions at specific focal planes where tissue delivery of STS was equivalent. This approach – quantifying apoptosis and cell death from cell counts – allows results to be plotted as cellular percentages and thus should be less dependent on cell density than measurements obtained from epifluorescence imaging. These cell-based metrics should be especially useful for gauging drug response profiles in heterogeneous primary tumor specimens. Our imaging approach can be extended by using tissue pre- and post-labeling reagents to gauge the response to any drug, small molecule or treatment.

Using confocal microscopy we were able to quantitatively compare the percentage of apoptosis ( $P_A$ ) and cell death ( $P_D$ ) at the STS-treated with those at the buffer regions (Fig. 5).  $P_A$  and  $P_D$  were consistently higher at the STS-treated regions than at the buffer regions. Since there is a wide interval between two drug channels, the intervening buffer regions provide within-sample and assay control regions to assess, e.g., background cell death from region to region across a tissue or biopsy slice. Heterogeneity in cell death within a sample or specimen can be assessed and controlled for by comparing treated and control regions in different areas of a tissue slice. We obtained the confocal images from two separate areas (top and bottom column boxes in Fig. 5) from the tissue slice to reduce the bias from our analysis and to include the importance of variability within a tissue sample. Our analysis revealed a surprising similarity between these two areas (top and bottom graphs). This multi-region analysis might potentially be useful to address tumor heterogeneity.

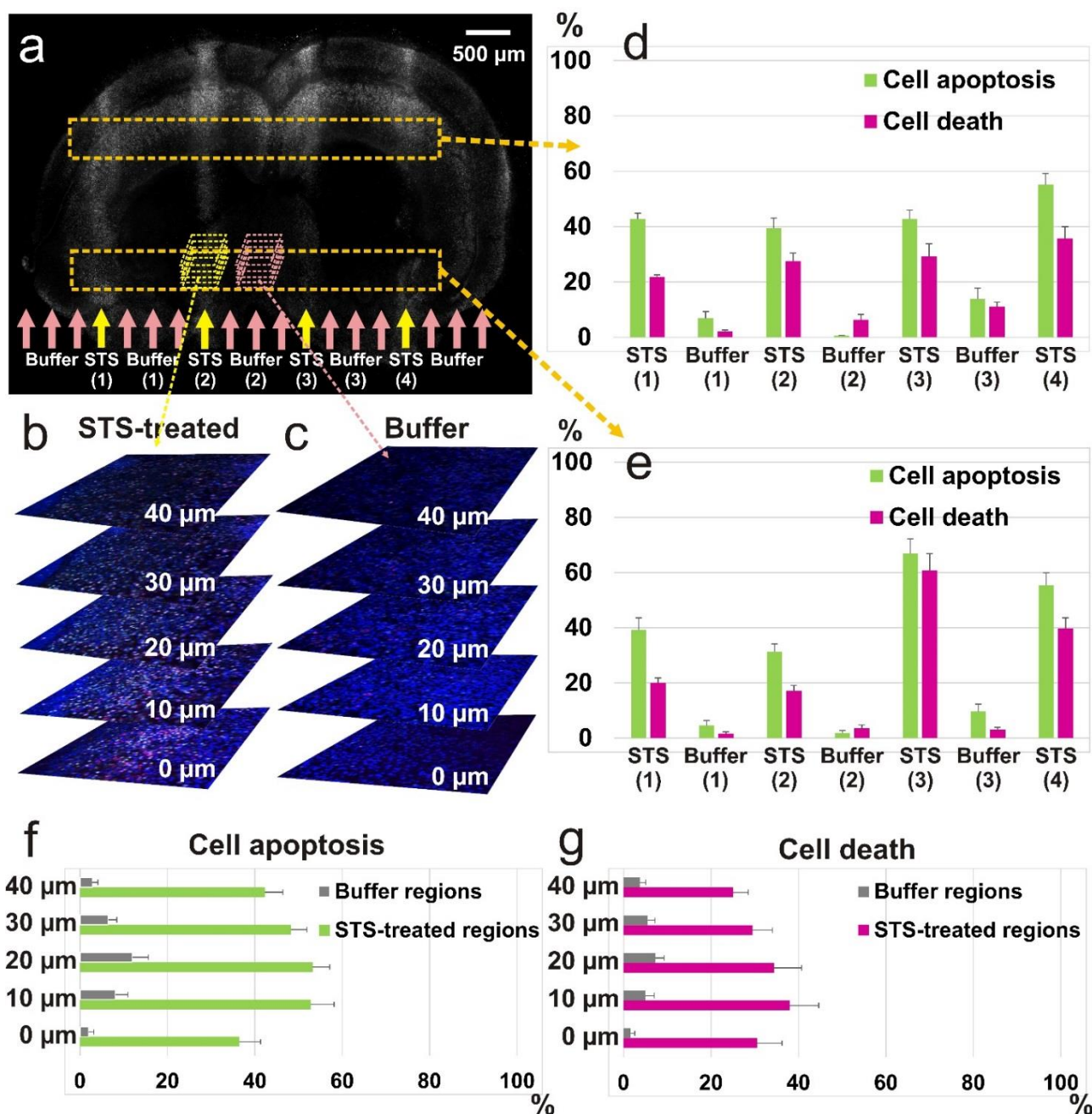


**Figure 5. Dose-dependent cell killing in intact tissue slice cultures quantified by confocal microscopy.** (a) Epifluorescence image (dead-cell staining) of a PI mouse brain slice after it is selectively treated with STS at four separate regions through four delivery channels (yellow arrows) for 24 hours, followed by apoptotic and dead cell staining. Four lanes of fluorescently labelled dead cells in the brain slice are visible in the STS-exposed areas. (b,c) Optical slices of STS-treated (b) and buffer (c) regions. Five optical slices are acquired at both regions of the tissue slice. Three fluorescence channels from a confocal microscope are used to detect cell nuclei (blue), cell apoptosis (green), and cell death (magenta). (d,e) Percentages of cell apoptosis and cell death across the slice (orange dashed boxes in Fig. 5a). Each error bar shows the standard error of mean. (f,g) Percentages of cell apoptosis (f) and cell death (g) at individual focal planes. Each error bar shows the standard error of mean.

Both epifluorescence and confocal microscopy can be used to quantify cellular responses to drug compounds. Epifluorescence microscopy with an automated stage can rapidly acquire images of a full tissue slice from the culture surface. However, the fluorescence signal from fluorescently-labeled cells may be variable when derived from brain or tissue regions that are variable in structure or cell density. Confocal microscopy, in contrast, allows optical sectioning of tissue slices to provide high spatial resolution, though is

substantially slower than simple epifluorescence imaging. Thus a hybrid imaging strategy with a customized imaging platform might provide the best combination of speed and accuracy to assess cellular response patterns in response to treatments.

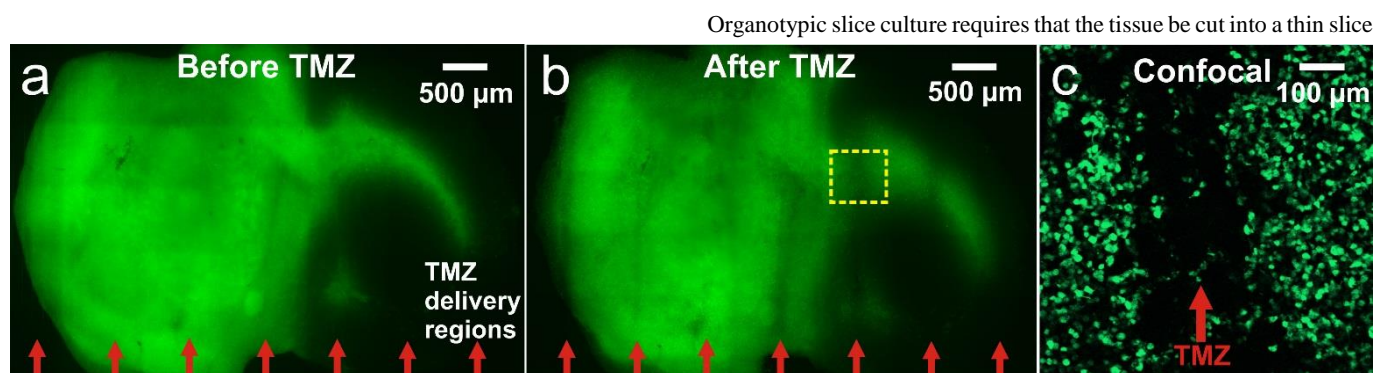


**Figure 6. Selective killing of GFP-labeled human GBM xenograft cells by TMZ in an intact xenograft slice culture (a,b)** Selective TMZ treatment on a GBM xenograft slice. The green areas show the GFP-labelled glioma cells within the slice. Seven parallel fluidic streams containing 1 mM TMZ (white-dashed arrows on panel a) and red arrows on panel b) were delivered to the slice with 3 buffer streams in between each of the two TMZ streams. The disappearance of GFP-labeled glioma cells was found after 48hr of TMZ delivery at the TMZ-exposed regions (b) compared to the image of the same slice before TMZ exposure (a). (c) A confocal image taken from the yellow-dashed box in (b) after 48hr TMZ exposure shows the loss of GFP-labeled glioma cells at the TMZ-exposed region in a spatially-defined manner.

### Regioselective drug exposure of a GBM xenograft slice

More effective cancer therapy with better treated outcomes will require better ways to accurately predict drug efficacy in individual cancer patients<sup>1</sup>. Our approach – multiplexed testing of large numbers of drugs on intact tissue slices – has the potential to identify more effective therapies for individual cancer patients. To demonstrate this potential, we used GBM mouse xenografts in which glioma cells were GFP-labeled to detect glioma cell death (since the glioma cells lose GFP and stop making GFP after cell death) after treatment with TMZ. TMZ is an alkylating agent that interferes with DNA replication, and is the current standard-of-care treatment for GBM patients. TMZ (1 mM) was delivered to GBM xenograft slice cultures in each of 7 delivery channels (buffer channels were filled with culture medium without TMZ) for 24 and 48 hours. Following drug exposure, GBM slice cultures on membranes were transferred to glass-bottom petri dishes for rinsing in PBS, fixing and imaging. Slices with 24 hrs of TMZ exposure did not show a significant response: GFP-labeled GBM cells remained in the drug exposure areas (as evaluated by epifluorescence microscopy). Treating GBM xenograft slice cultures for 48 hrs, in contrast, significantly increased cell killing as evidenced by the loss of GFP-labeled GBM cells to TMZ as shown in Fig. 6a-b. Our results show that glioma cell loss formed “shadow” lanes over TMZ delivery channels as compared with tissue prior to drug exposure or over channels perfused with culture medium lacking TMZ (Fig. 6b); the “shadow” lanes are not fully dark because TMZ did not penetrate the full depth of the volume occupied by GFP-labeled cells. Further, we analyzed the TMZ and medium-perfused regions by quantifying the reduction of fluorescence intensity before and after the treatment. To calculate average intensity values, the TMZ-exposed regions were selected at the areas over TMZ delivery channels, and the buffer-exposed control regions (without TMZ) were selected at the areas over control channels. We found a 31.2% average reduction in fluorescence intensity (S.D. = 8.6) at the TMZ-exposed regions, compared to a 12.8% (S.D. = 5) at the control regions. As expected, confocal imaging over TMZ-exposed regions/channels (Fig. 6c) confirmed the TMZ-dependent loss of GFP-labeled cells.

### Potential use of core needle biopsy tissues

(~200–400μm) such that mass transport of nutrients and oxygen is not diffusion-limited (i.e., it must be sufficiently small in at least one dimension). In this paper, we have used tissue slices to demonstrate our device because the thickness of the slices can be finely controlled by a Vibratome tissue slicer. We have also tested core tissue biopsies extracted from a mouse liver using a 600 μm-diam. biopsy tool and demonstrated that it is feasible to combine the use of core biopsy tissues with our microfluidic device (Supplementary Fig. 13). Core biopsy is a rapid process for obtaining intact tissues and a commonly used technique for establishing diagnosis and monitoring cancer tissue progression. The direct use of core tissue biopsies for drug screening would allow for the identification of effective drug compounds without the need of additional surgical processes on patients<sup>35</sup>.

### Conclusions

Our microfluidic platform has two key features that overcome current limitations of high-throughput cancer drug screening on intact tissues: 1) the coupling of organotypic slice culture with a microfluidic drug delivery device, which is used to perfuse the intact tissue slices through a removable PTFE membrane; and 2) the adaptation of this approach to a familiar multi-well plate format, enabling multiplexed fluid routing and facilitating tissue handling and imaging for assessing tissue drug response patterns. With these features, our platform improves upon existing models for screening chemotherapeutic drug activity and allows the generation of response data in a time frame that can potentially guide decision-making for the initial phases of cancer therapy.

### References

1. Provocative Questions, <http://provocativequestions.nci.nih.gov/rfa>.
2. C. B. T. R. o. t. U. S. (CBTRUS), *CBTRUS Statistical Report: Primary Brain and Central Nervous System Tumors Diagnosed in Eighteen States in 2002–2006*, 2009.
3. C. W. Brennan, R. G. Verhaak, A. McKenna, B. Campos, H. Noshmeh, S. R. Salama, S. Zheng, D. Chakravarty, J. Z. Sanborn and S. H. Berman, *Cell*, 2013, 155, 462–477.
4. M. E. Hegi, L. Liu, J. G. Herman, R. Stupp, W. Wick, M. Weller, M. P. Mehta and M. R. Gilbert, *Journal of Clinical Oncology*, 2008, 26, 4189–4199.

5. Y. Sun, J. Campisi, C. Higano, T. M. Beer, P. Porter, I. Coleman, L. True and P. S. Nelson, *Nature medicine*, 2012, 18, 1359-1368.
6. E. S. Nakasone, H. A. Askautrud, T. Kees, J.-H. Park, V. Plaks, A. J. Ewald, M. Fein, M. G. Rasch, Y.-X. Tan and J. Qiu, *Cancer cell*, 2012, 21, 488-503.
7. F. Pampaloni, E. G. Reynaud and E. H. Stelzer, *Nature reviews Molecular cell biology*, 2007, 8, 839-845.
8. D. Wlodkowic and J. M. Cooper, *Current opinion in chemical biology*, 2010, 14, 556-567.
9. D. W. Infanger, M. E. Lynch and C. Fischbach, *Annual review of biomedical engineering*, 2013, 15, 29-53.
10. D. Hanahan and Robert A. Weinberg, *Cell*, 2011, 144, 646-674.
11. H. L. Haas, B. Schaerer and M. Vosmansky, *J. Neurosci. Methods*, 1979, 1, 323-325.
12. F. Merz, F. Gaunitz, F. Dehghani, C. Renner, J. Meixensberger, A. Gutenberg, A. Giese, K. Schopow, C. Hellwig and M. Schäfer, *Neuro-oncology*, 2013, 15, 670-681.
13. I. A. M. de Graaf, P. Olinga, M. H. de Jager, M. T. Merema, R. de Kanter, E. G. van de Kerkhof and G. M. M. Groothuis, *Nat. Protocols*, 2010, 5, 1540-1551.
14. V. Vaira, G. Fedele, S. Pyne, E. Fasoli, G. Zadra, D. Bailey, E. Snyder, A. Faverversani, G. Coggi, R. Flavin, S. Bosari and M. Loda, *Proceedings of the National Academy of Sciences*, 2010, 107, 8352-8356.
15. J. Noraberg, F. R. Poulsen, M. Blaabjerg, B. W. Kristensen, C. Bonde, M. Montero, M. Meyer, J. B. Gramsbergen and J. Zimmer, *Current drug targets. CNS and neurological disorders*, 2005, 4, 435-452.
16. B. P. Murry, B. E. Blust, A. Singh, T. P. Foster and D. Marchetti, *Journal of Cellular Biochemistry*, 2006, 97, 217-225.
17. A. Blake, T. Pearce, N. Rao, S. Johnson and J. Williams, *Lab on a Chip*, 2007, 7, 842-849.
18. Y. Huang, J. C. Williams and S. M. Johnson, *Lab on a Chip*, 2012, 12, 2103-2117.
19. H. Haas, B. Schaerer and M. Vosmansky, *Journal of neuroscience methods*, 1979, 1, 323-325.
20. L. Stoppini, P.-A. Buchs and D. Muller, *Journal of neuroscience methods*, 1991, 37, 173-182.
21. S. Charati and S. Stern, *Macromolecules*, 1998, 31, 5529-5535.
22. A. R. Parrish, A. J. Gandolfi and K. Brendel, *Life sciences*, 1995, 57, 1887-1901.
23. J. Noraberg, F. R. Poulsen, M. Blaabjerg, B. W. Kristensen, C. Bonde, M. Montero, M. Meyer, J. B. Gramsbergen and J. Zimmer, *Current Drug Targets-CNS & Neurological Disorders*, 2005, 4, 435-452.
24. N. Parajuli and W. Doppler, *In Vitro Cellular & Developmental Biology-Animal*, 2009, 45, 442-450.
25. H. Wakimoto, S. Kesari, C. J. Farrell, W. T. Curry, C. Zaupa, M. Aghi, T. Kuroda, A. Stemmer-Rachamimov, K. Shah and T.-C. Liu, *Cancer research*, 2009, 69, 3472-3481.
26. S. A. Mikheeva, A. M. Mikheev, A. Petit, R. Beyer, R. G. Oxford, L. Khorasani, J.-P. Maxwell, C. A. Glackin, H. Wakimoto and I. González-Herrero, *Mol Cancer*, 2010, 9, 10.1186.
27. H. Hama, H. Kurokawa, H. Kawano, R. Ando, T. Shimogori, H. Noda, K. Fukami, A. Sakaue-Sawano and A. Miyawaki, *Nature neuroscience*, 2011, 14, 1481-1488.
28. S. Kalyanasundaram, V. Calhoun and K. Leong, *American Journal of Physiology-Regulatory, Integrative and Comparative Physiology*, 1997, 273, R1810-R1821.
29. C. J. Choi and B. T. Cunningham, *Lab on a Chip*, 2007, 7, 550-556.
30. C.-H. Hsu, C. Chen and A. Folch, *Lab Chip*, 2004, 4, 420-424.
31. V. Sunkara, D.-K. Park, H. Hwang, R. Chantiwas, S. A. Soper and Y.-K. Cho, *Lab on a Chip*, 2011, 11, 962-965.
32. M. J. Lee, A. S. Ye, A. K. Gardino, A. M. Heijink, P. K. Sorger, G. MacBeath and M. B. Yaffe, *Cell*, 2012, 149, 780-794.
33. A. Gescher, *General Pharmacology: The Vascular System*, 1998, 31, 721-728.
34. J.-Y. Koh, M. B. Wie, B. J. Gwag, S. L. Sensi, L. M. Canzoniero, J. Demaro, C. Csernansky and D. W. Choi, *Experimental neurology*, 1995, 135, 153-159.
35. S. M. Hattersley, C. E. Dyer, J. Greenman and S. J. Haswell, *Lab on a Chip*, 2008, 8, 1842-1846.